9

Recent Advances in Modeling Axisymmetric Swirl and Applications for Enhanced Heat Transfer and Flow Mixing

Sal B. Rodriguez[1] and Mohamed S. El-Genk[2]
[1]*Sandia National Laboratories,*
[2]*University of New Mexico*
USA

1. Introduction

The concept of enhanced heat transfer and flow mixing using swirling jets has been investigated for nearly seven decades (Burgers, 1948; Watson and Clarke, 1947). Many practical applications of swirling jets include combustion, pharmaceuticals, tempering of metals, electrochemical mass transfer, metallurgy, propulsion, cooling of high-power electronics and computer chips, atomization, and the food industry, such as improved pizza ovens. Recently, swirling jet models have been applied to investigate heat transfer and flow mixing in nuclear reactors, including the usage of swirling jets in the lower plenum (LP) of generation-IV very high temperature gas-cooled reactors (VHTRs) to enhance mixing of the helium coolant and eliminate the formation of hot spots in the lower support plate, a safety concern (Johnson, 2008; Kim, Lim, and Lee, 2007; Laurien, Lavante, and Wang, 2010; Lavante and Laurien, 2007; Nematollahi and Nazifi, 2007; Rodriguez and El-Genk, 2008a, b, c, and d; Rodriguez, Domino, and El-Genk, 2010; Rodriguez and El-Genk, 2010a and b; Rodriguez and El-Genk, 2011).

There are many devices and processes for generating vortex fields to enhance flow mixing and convective heat transfer. Figure 1 shows a static helicoid device that can be used to generate vortex fields based on the swirling angle, θ. Recent advances in swirling jet technology exploit common characteristics found in axisymmetric vortex flows, and these traits can be employed to design the vortex flow field according to the desired applications; among these are the degree of swirl (based on the swirl number, S) and the spatial distributions of the radial, azimuthal, and axial velocities.

For a 3D helicoid, the vortex velocity in Cartesian coordinates can be approximated as:

$$\vec{V}_o(x,y,z) = u_o \sin(2\pi y)\vec{i} - u_o \sin(2\pi x)\vec{j} + w_o\vec{k} \quad (1)$$

For a jet with small radius r, the above velocity distribution can be represented in cylindrical coordinates as

$$v_\theta(r) = u_o \sin(\pi r) \quad (2)$$

and

$$w_z(r) = w_o \,. \tag{3}$$

Whereas there are about a dozen or so definitions of the swirling number S, we define it as a pure geometric entity, consistent with various investigators in the literature (Arzutug and Yapici, 2009; Bilen *et al*. 2002; Kerr and Fraser, 1965; Mathur and MacCallum, 1967):

$$S = \frac{2}{3}\tan(\theta) \tag{4}$$

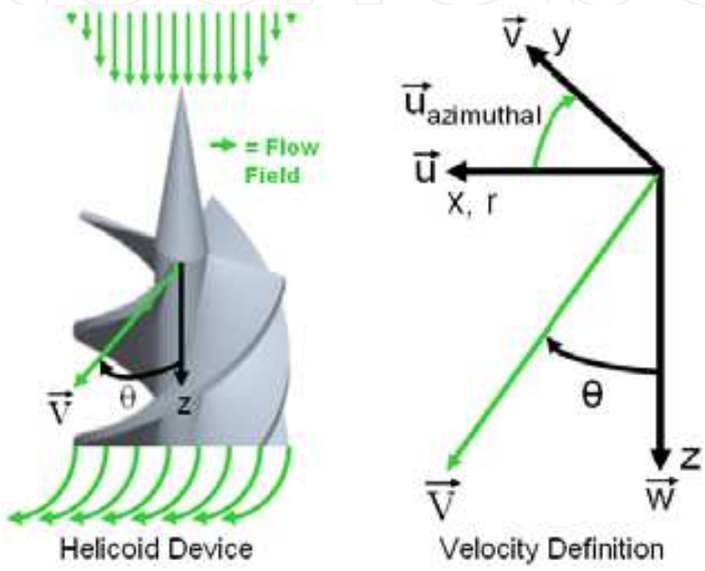

Fig. 1. Helicoid swirl device and associated velocity distribution

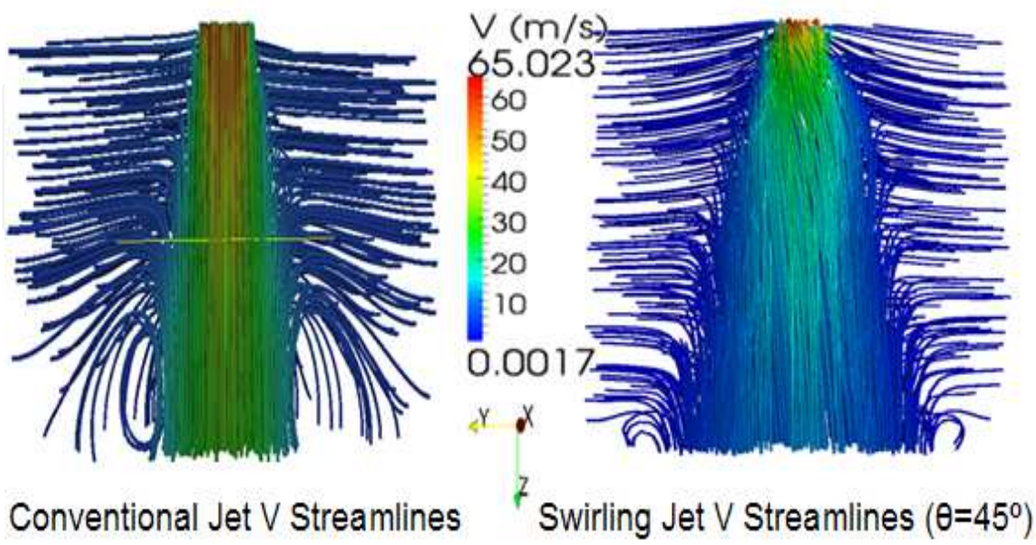

Fig. 2. Comparison of conventional vs. swirling jet velocity streamlines

Increasing S has been shown to increase the entrainment of the surrounding fluid (K_e) linearly (Kerr and Fraser, 1965) as:

$$K_e = 0.35 + 1.4S \, . \tag{5}$$

As a result of the increased entrainment, mixing, and turbulence, a swirling jet has a wider core diameter than a conventional impinging jet, as shown in Figure 2. Further, the azimuthal velocity of the helicoid vortex increases as S increases,

$$\frac{v_{\theta,0}}{V_0} = \frac{1}{\left(1 + \frac{4}{9S^2}\right)^{\frac{1}{2}}} \tag{6}$$

while the axial velocity decreases (Rodriguez and El-Genk, 2010b),

$$\frac{w_{z,0}}{V_0} = \frac{2}{3S} \frac{1}{\left(1 + \frac{4}{9S^2}\right)^{\frac{1}{2}}}. \tag{7}$$

V_0 is the velocity at the jet exit when no swirling occurs (conventional jet).

2. Vortex modeling

For this discussion, the broad field of turbulent vortex flows is narrowed down to swirling Newtonian fluid jets that are axisymmetric and incompressible. These vortices have been studied in many coordinates. A rather "unnatural" selection is Cartesian coordinates, as the flow field rotates about the axisymmetric axis, which is generally selected as the z coordinate. Therefore, the axisymmetric vortex flow is symmetric about the z axis as the flow rotates in the azimuthal direction, and continues to expand in the z direction.

As noted in Figure 2, both impinging and swirling jets have the same source diameter and expand into an open domain. While the conventional jet experiences no azimuthal rotation, the swirling jet with $\theta = 45^o$ has a strong rotational flow component. Note that the swirling jet has a wider jet core diameter, a higher degree of entrainment of surrounding fluid, and its azimuthal rotation causes more fluid mixing than the conventional impinging jet. Because part of the axial momentum in the swirling jet is converted to azimuthal momentum, the axial velocity component decays much faster than for the conventional jet.

Vortex research in Cartesian coordinates includes the Green-Taylor vortex (Taylor and Green, 1937) and the helicoid vortex discussed herein (Rodriguez and El-Genk, 2008a, 2010b and d). Various researchers selected spherical coordinates (Gol'Dshtik and Yavorskii, 1986; Hwang and Chwang, 1992; Tsukker, 1955), but the vast majority of the research found in the literature is in cylindrical coordinates (Aboelkassem, Vatistas, and Esmail, 2005; Batchelor, 1964; Burgers, 1948; Chepura, 1969; Gortler, 1954; Lamb, 1932; Loitsyanskiy, 1953; Martynenko, 1989; Newman, 1959; Rankine, 1858; Rodriguez and El-Genk, 2008a, 2010b and d; Sullivan, 1959; Squire, 1965). Cylindrical coordinates are chosen primarily due to its geometric simplicity and excellent mapping of the vortex behavior onto a coordinate system—in particular, as a 3D vortex spins azimuthally, stretching about the z axis, the vortex velocity field engulfs a cylindrical geometry. Certainly, conical coordinates could be

used, but they are not as convenient to manipulate mathematically. Indeed, as the vortex expands, forming a 3D cone, care needs to be taken such that the swirl field is not so large that it generates a field with an angle that is larger than the conical coordinate system.
Consider a cylindrical coordinate system with r, θ, and z as the radial, azimuthal, and axial components, as defined in Figure 1. For 3D, steady state, negligible gravitational effect, incompressible, Newtonian fluids with symmetry about the z axis (axisymmetry), the momentum and conservation of mass equations are given as:

$$u\frac{\partial u_r}{\partial r}-\frac{\mathrm{v}^2}{r}+w\frac{\partial u}{\partial z}=-\frac{1}{\rho}\frac{\partial p}{\partial r}+\nu\left(\frac{\partial^2 u}{\partial r^2}+\frac{1}{r}\frac{\partial u}{\partial r}-\frac{u}{r^2}+\frac{\partial^2 u}{\partial z^2}\right) \tag{8}$$

$$u\frac{\partial \mathrm{v}}{\partial r}+\frac{\mathrm{v}u}{r}+w\frac{\partial \mathrm{v}}{\partial z}=\nu\left(\frac{\partial^2 \mathrm{v}}{\partial r^2}+\frac{1}{r}\frac{\partial \mathrm{v}}{\partial r}-\frac{\mathrm{v}}{r^2}+\frac{\partial^2 \mathrm{v}}{\partial z^2}\right) \tag{9}$$

$$u\frac{\partial w}{\partial r}+w\frac{\partial w}{\partial z}=-\frac{1}{\rho}\frac{\partial p}{\partial z}+\nu\left(\frac{\partial^2 w}{\partial r^2}+\frac{1}{r}\frac{\partial w}{\partial r}+\frac{\partial^2 w}{\partial z^2}\right) \tag{10}$$

$$\frac{\partial u}{\partial r}+\frac{u}{r}+\frac{\partial w}{\partial z}=0 \tag{11}$$

An inspection of the literature over the past 150 years shows that the above equations are generally the departure point for generating analytic solutions for axisymmetric swirling flows (vortices) (Aboelkassem, Vatistas, and Esmail, 2005; Batchelor, 1964; Burgers, 1948; Chepura, 1969; Gortler, 1954; Lamb, 1932; Loitsyanskiy, 1953; Martynenko, 1989; Newman, 1959; Rankine, 1858; Rodriguez and El-Genk, 2010b; Sullivan, 1959; Squire, 1965).

3. Helicoid swirl modeling

Helicoids for the generation of swirling-flow fields may be produced by various methods. One method is via a geometrical specification of a static, swirl device that consists of helicoidal surfaces, and another is a mathematical description of a swirl boundary condition (BC) that reproduces the flow field. It has been reported in the literature and confirmed herein that if a computational fluid mechanics (CFD) code does not have a swirl boundary option, it would be customary to develop the geometry for a swirl device and then mesh it (Duwig *et al.* 2005; Fujimoto, Inokuchi, and Yamasaki, 2005; Garcia-Villalba, Frohlich, and Rodi, 2005; Rodriguez and El-Genk, 2008a, b, c, and d; Rodriguez, Domino, and El-Genk, 2010; Rodriguez and El-Genk, 2010a and b; Rodriguez and El-Genk, 2011). Several static swirl devices are shown in Figure 3 (Huang, 1996; Huang and El-Genk, 1998; Larocque, 2004; Rodriguez and El-Genk, 2010a and b; Rodriguez and El-Genk, 2011). The swirl device considered in this chapter consists of a sharp cone that surrounds four helical surfaces off-set by 90° and spiral symmetrically around the cylinder (Figure 4, LHS). Because the swirling device is static, the fluid flows around the helicoid surfaces, producing a swirling motion as it travels around the surfaces.
Deciding on a particular swirl angle *a priori* for the swirling device, and then meshing its geometry, is computationally-intensive and time consuming, not to mention that it is a tedious, error-prone, and expensive process. Instead, as will be shown *a posteriori*, having a

closed form, mathematical formulation for the swirling field not only simplifies the computation requirements but also yields significant insights concerning the behavior of the velocity fields and their impact on heat transfer.

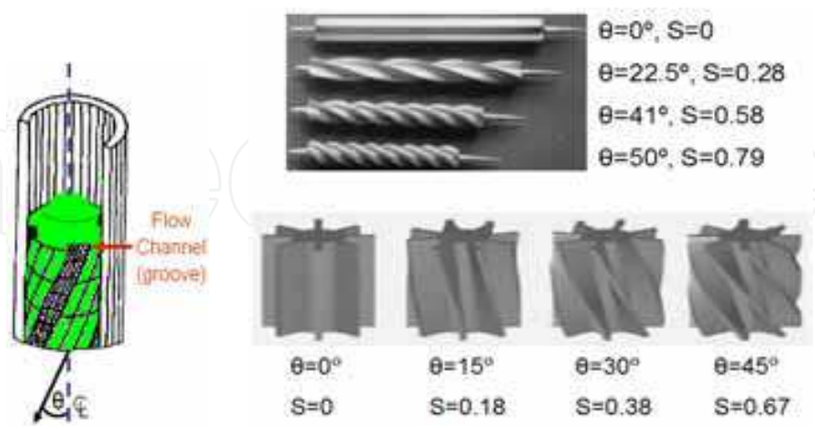

Fig. 3. Various Swirl Devices Found in the Literature (Huang, 1996; Huang and El-Genk, 1998; Larocque, 2004; Rodriguez and El-Genk, 2010a and b; Rodriguez and El-Genk, 2011)

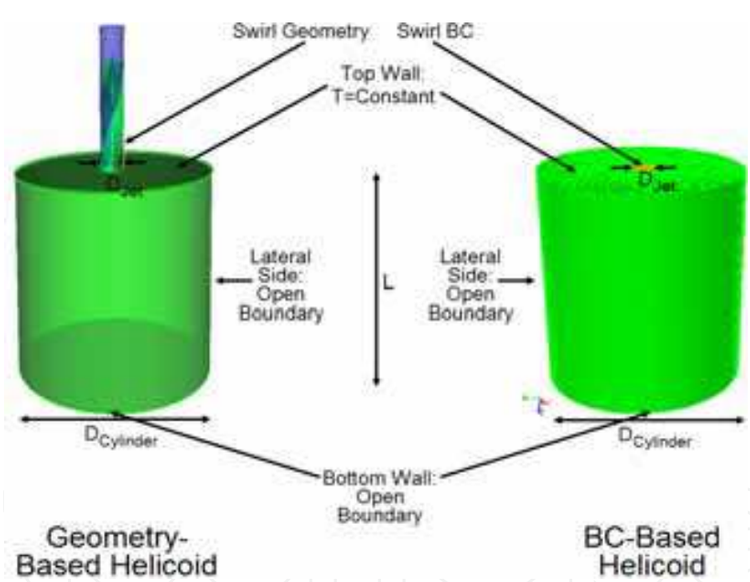

Fig. 4. Comparison of Geometric and BC Swirl Models

Now, once a mathematical swirl formulation is derived, it is a straightforward matter to apportion the jet velocity fields such that a given swirl angle is uniquely specified (Equations 4, 6, and 7). As a result, a mathematically-generated velocity field with no helicoid surfaces (i.e. just swirl BCs) can very closely approximate the swirl fields of the geometric helicoid devices shown in Figure 1. To demonstrate this, two meshes are shown: one with a geometric swirl device and the other with swirl BCs (see Figure 4). The CFD computation for both meshes has the same S.

A comparison of both models shows that the total velocity vector streamlines are essentially indistinguishable, as shown in Figure 5. The azimuthal velocity compared in Figure 6, again shows that the velocity streamlines are fairly identical. This methodology results in

significant savings in the meshing and computational effort, especially because the helicoid geometry requires finite elements that are about four times smaller than the rest of the model, and further, the time step is dominated by the smallest finite element.

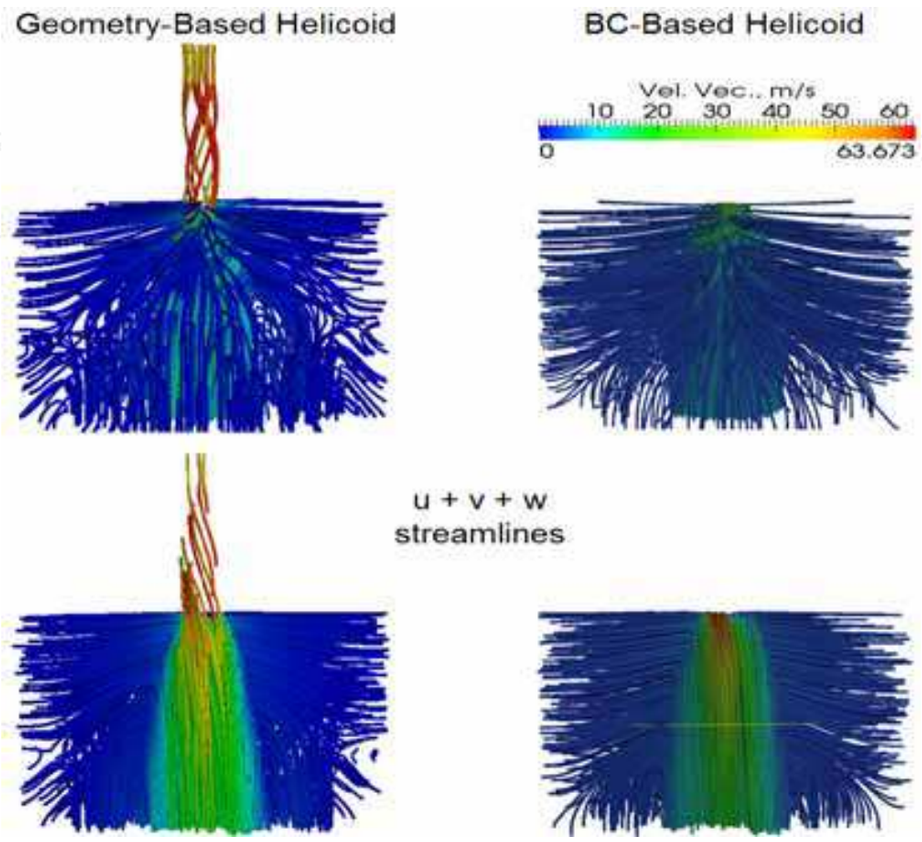

Fig. 5. Comparison of the Geometric and BC Swirl Models: U + V + W Streamlines

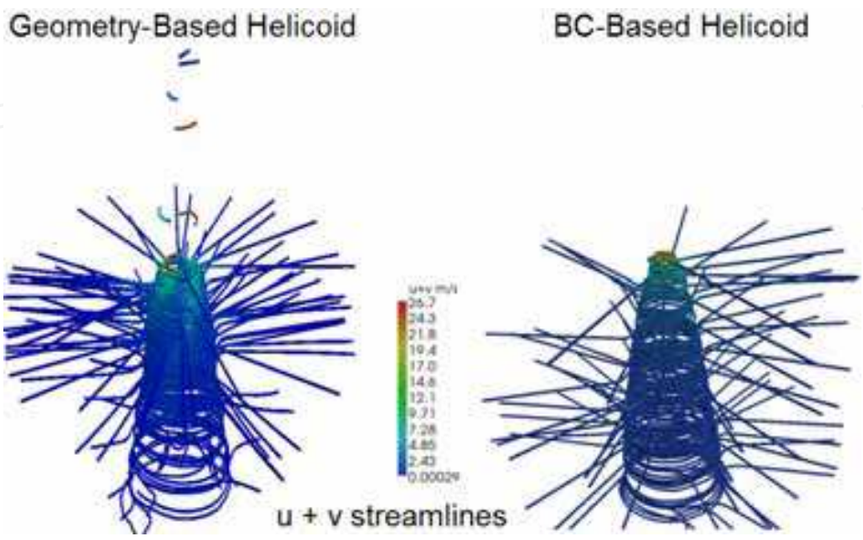

Fig. 6. Comparison of the Geometric and BC Swirl Models: Azimuthal Velocity Streamlines

4. Swirling jet strongest domain

The results of CFD calculations with swirl BCs agree with both theory and experimental data for weak to intermediate S, showing that the peak azimuthal velocity v_θ decays as $1/z^2$, while the peak axial velocity w decays as $1/z$ (Blevins, 1992; Billant *et al*. 1998; Chigier and Chervinsky, 1967; Gortler, 1954; Loitsyanskiy, 1953; Mathur and MacCallum, 1967). This issue, defined as "swirl decay", was first reported by Loitsyanskiy. In particular, as z becomes large, the peak azimuthal velocity decays much faster. That is,

$$w = \frac{C_1}{z} \tag{12}$$

and

$$v_\theta = \frac{C_2}{z^2}. \tag{13}$$

Based on a curve-fit of the reported data in the literature (Blevins, 1992), it is possible to obtain $C_1 = -2.6S^3+12S^2+19S+12$, while the reported value in the literature for $C_2 \sim 4$ to 11, and may be a function of S (Blevins, 1992).

Because the azimuthal velocity for a swirling jet decays faster than the axial velocity, there is a point, z*, where for $z \le z^*$, $w \le v_\theta$. Setting $z = z^*$ and solving for $v_\theta(z^*) = w(z^*)$, yields:

$$z^* = \frac{C_2}{C_1} = \frac{C_2}{-2.6S^3+12S^2+19S+12} \tag{14}$$

Clearly, the magnitude of z* that maximizes the azimuthal momentum vs. the axial momentum depends strongly on the value of S. For example, for S = 0.2 and 0.6, z* = 1.3 and 2.6, respectively. Therefore, if the purpose is to optimize the flow mixing and convective heat transfer caused by swirl, a guideline is to have $w \le v_\theta$, such that Equation 14 is satisfied.

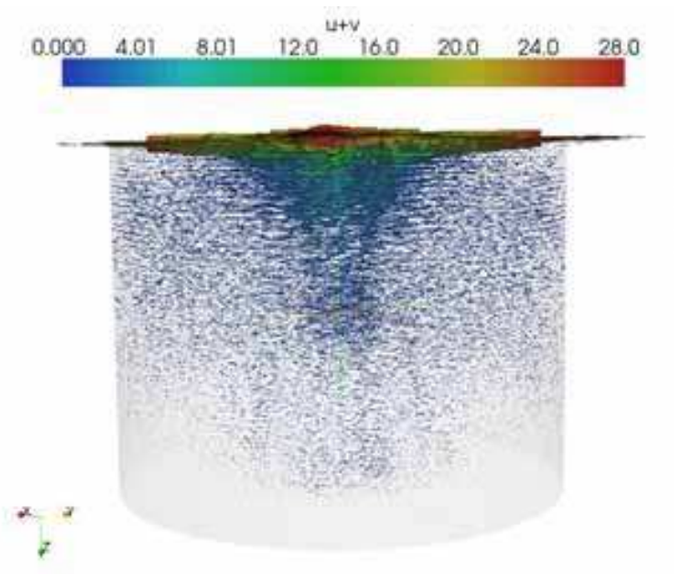

Fig. 7. Fast Decay of the Azimuthal Velocity

A consequence of the azimuthal rotation is that swirling jets experience swirl decay (see Figure 7). Therefore, there is a point beyond which the azimuthal velocity will decay to a degree whereby it no longer significantly impacts the flow field. This factor is crucial in the design of swirling jets, and in any applications that employ swirling jets for enhancing heat and mass transfer, combustion, and flow mixing.

5. Impact of S on the Central Recirculation Zone

As the azimuthal velocity increases and exceeds the axial velocity, a low pressure region prevails near the jet exit where the azimuthal velocity is the highest. The low pressure causes a reversal in the axial velocity, thus producing a region of backflow. Because the azimuthal velocity forms circular planes, and the reverse axial velocity superimposes onto it, the net result is a pear-shaped central recirculation zone (CRZ). From a different point of view, for an incompressible swirling jet, as S increases, the azimuthal momentum increases at the expense of the axial momentum (see Equations 6 and 7). This is consistent with the data in the literature (Chigier and Chervinsky, 1967).
The CRZ formation results in a region where vortices oscillate, similar to vortex shedding for flow around a cylinder. The enhanced mixing associated with the CRZ is attributable to the back flow in the axial direction; in particular, the back flow acts as a pump that brings back fluid for further mixing. The CRZ vortices tend to recirculate and entrain fluid into the central region of the swirling jet, thus enhancing mixing and heat transfer within the CRZ.

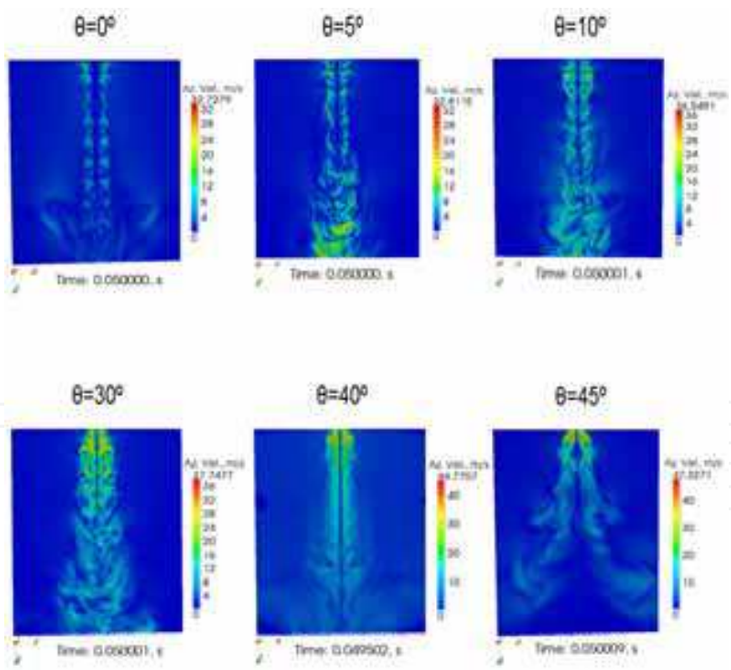

Fig. 8. Effect of Swirl Angle on the Azimuthal Velocity

The Fuego CFD code was used to compute the flow fields shown in Figures 8 through 10 (Fuego, 2009). Figure 8 shows the effect of the swirl angle on the azimuthal flow for an unconfined swirling jet. Figure 9 shows the velocity vector, azimuthal velocity, and the axial velocity for a weak swirl, while Figure 10 shows the same, but for moderate to strong swirl.

Note the dramatic changes that occur in the axial and azimuthal velocity distributions as the CRZ forms – the most significant change occurs in the z-direction, which is the axis normal to the jet flow. For example, for θ = 40º (no CRZ), the maximum azimuthal velocity at the bottom of the domain along the z axis is 15 m/s. But, when the CRZ forms at θ = 45º, the maximum azimuthal velocity is essentially 0. The same effect can be observed for the axial velocity for pre- and post-CRZ velocity distributions. Note that the region near the bottom of the z-axis for θ = 45º forms a stagnant cone that is surrounded by azimuthal flow moving around the cone at ~15 m/s, and likewise for the axial velocity.

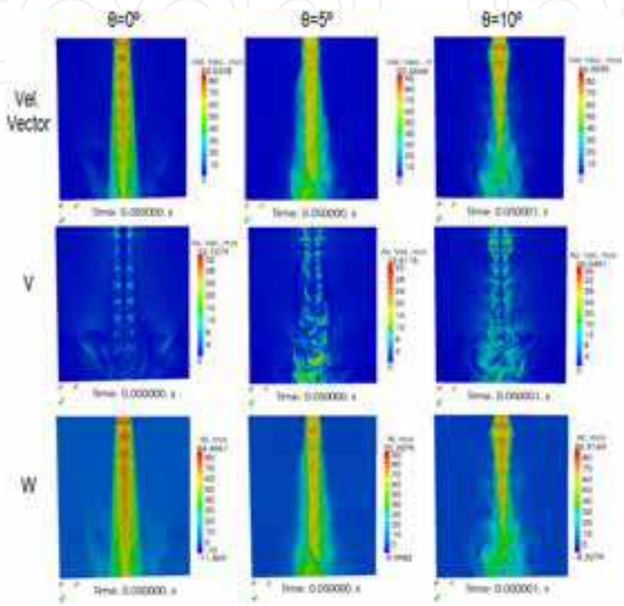

Fig. 9. Various Velocities for a Small Swirl Angle

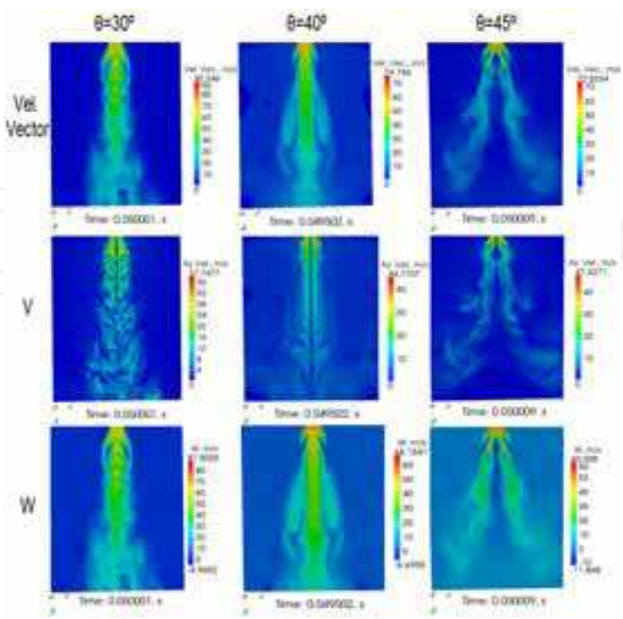

Fig. 10. Various Velocities for Moderate to Strong Swirl Angle

From Figure 10, it is quite evident that the CRZ acts as a "solid" body around which the strong swirling jet flows. This is important, as the CRZ basically has two key impacts on the flow domain: 1) it diminishes the momentum along the flow axis and 2) both the axial and azimuthal velocities drop much faster than $1/z$ and $1/z^2$, respectively. *Therefore, whether a CRZ is useful in the design problem or not depends on what issue is being addressed. In particular, if it is desirable that a hot fluid be dispersed as rapidly as possible, then the CRZ is useful because it more rapidly decreases the axial and azimuthal velocities of a swirling jet. However, if having a large conical region with nearly zero axial and azimuthal velocity is undesirable, then it is recommended that* $S < 0.67$. In the case of the VHTR, the support plate temperatures decrease as S increases; an S = 2.49 results in the lowest temperatures.

6. Impact of Re and S on mixing and heat transfer

In this section, two models are discussed in order to address this issue: (1) a cylindrical domain with a centrally-positioned swirling air jet and (2) a quadrilateral domain with six swirling jets. The single-jet model and its results are presented first, followed by the six-jet model discussion and results.

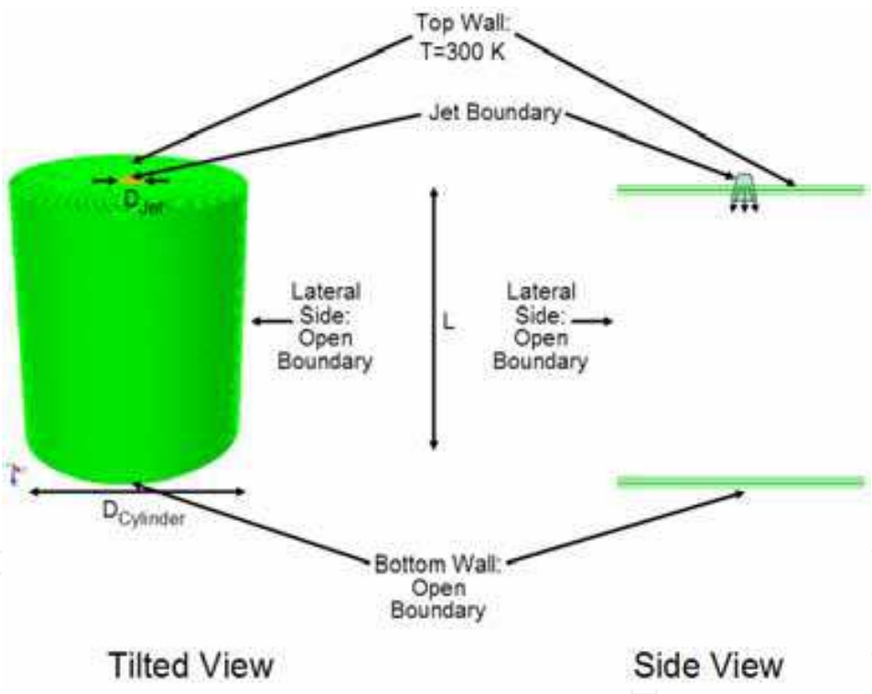

Fig. 11. Cylinder with a Single Swirling-Jet Boundary

Both models are run on the massively-parallel Thunderbird machine at Sandia National Laboratories (SNL). The initial time step used is 0.1 μs, and the maximum Courant-Friedrichs-Lewy (CFL) condition of 1.0, which resulted in a time step on the order of 1 μs. The simulations are typically run for about 0.05 to several seconds of transient time. Both models are meshed using hexahedral elements with the CUBIT code (CUBIT, 2009). The temperature-dependent thermal properties for air are calculated using a CANTERA XML input file that is based on the Chapman-Enskog formulation (Bird, Steward, and Lightfoot, 2007). Finally, both models used the dynamic Smagorinsky turbulence scheme (Fuego, 2009; Smagorinsky, 1963).

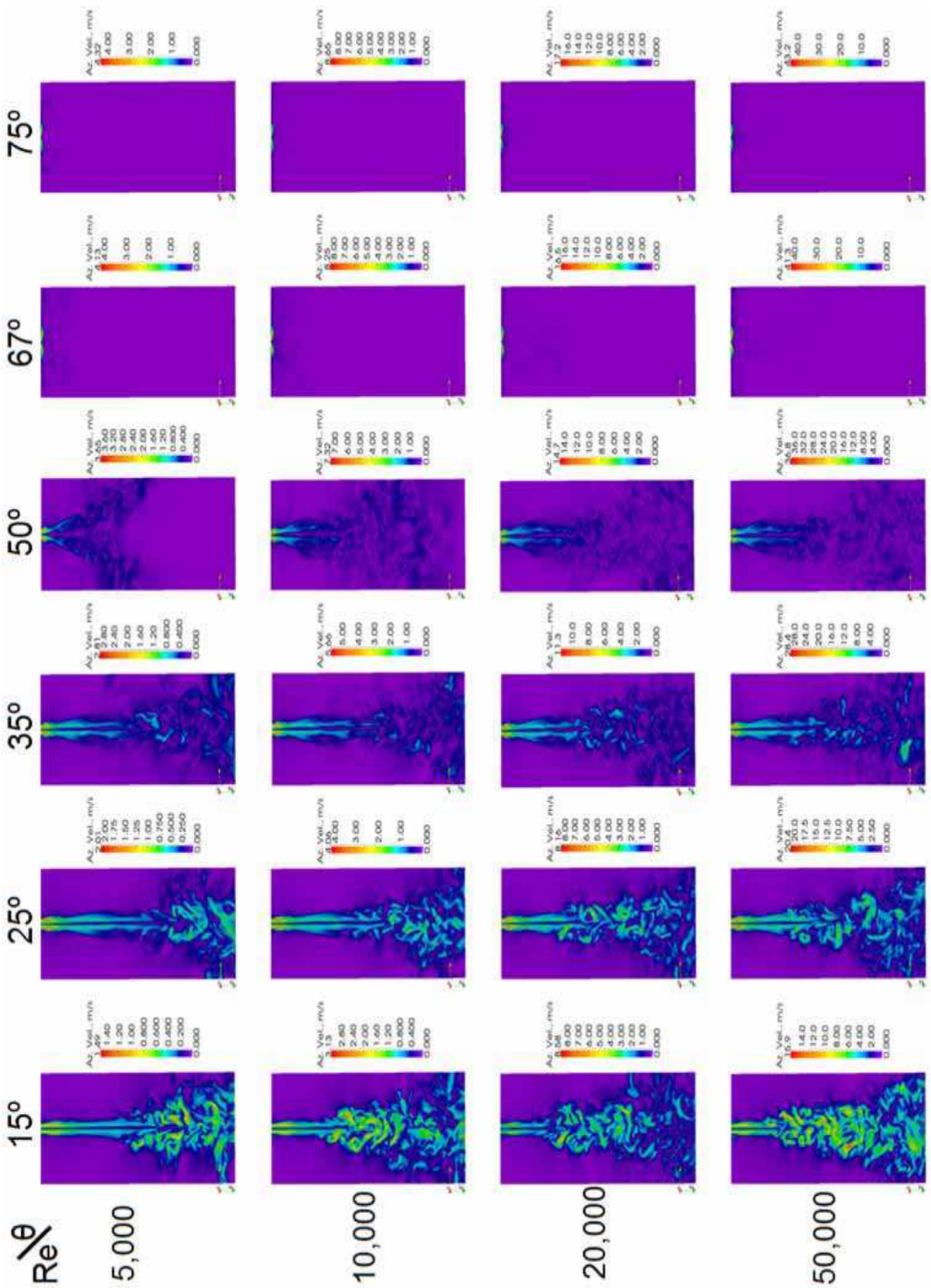

Fig. 12. Impact of Re and θ on Azimuthal Velocity Field

The single-jet computation domain consisted of a right cylinder that enclosed a centrally-positioned single, unbounded, swirling air jet (Figure 11). The meshed computational domain consisted of 1 million hexahedral elements. The top surface (minus the jet BC) is modeled as a wall, while the lateral and bottom surfaces of the cylindrical domain are open boundaries.

Figure 12 shows the effect of the swirl angle and Reynolds number (Re) on the azimuthal velocity field for θ = 15, 25, 35, 50, 67, and 75° (S =0.18, 0.31, 0.79, 1.57, and 2.49, respectively). Re was 5,000, 10,000, 20,000, and 50,000. For fixed S, as Re increases the azimuthal velocity turbulence increases, and the jet core becomes wider. For a fixed Re, as S increases the azimuthal velocity increases. The figure also shows the strong impact the CRZ formation has on how far the swirling jet travels before it disperses. *Thus, as soon as the CRZ appears, the azimuthal velocity field does not travel as far, even as Re is increased substantially. In other words, although Re increased 10-fold as shown in the figure, its impact was not as great on the flow field as that of S once the CRZ developed.*

The computational mesh used for the quadrilateral 3D domain for the six circular, swirling air jets is shown in Figure 13. The air temperature and approach velocity in the z direction for the jets was 300 K and 60 m/s. The numerical mesh grid in the computation domain consisted of 2.5×10^5 to 5×10^6 hexahedral elements.

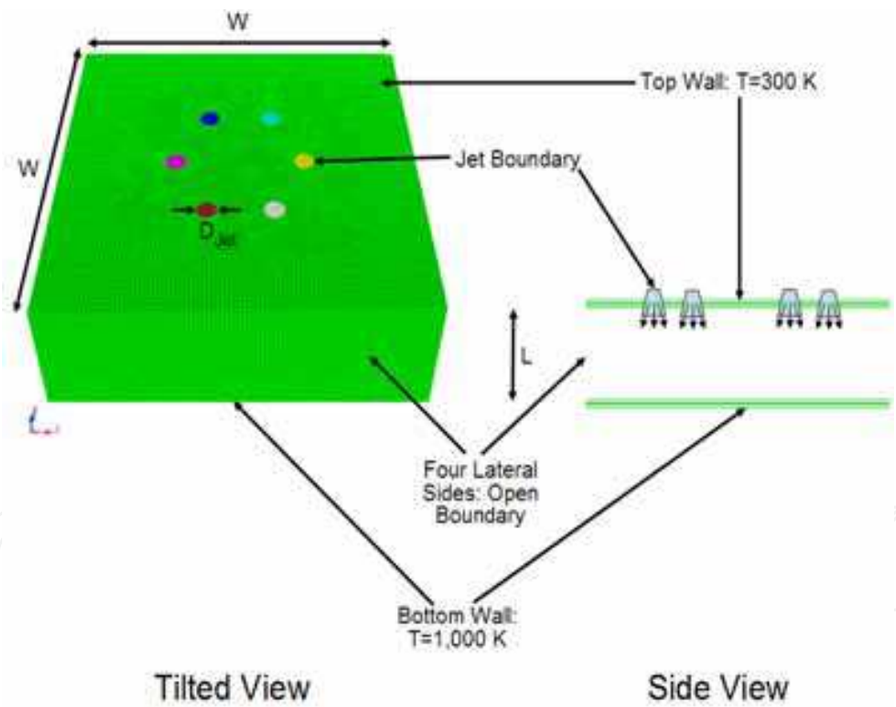

Fig. 13. Quadrilateral with Six Swirling-Jet Boundaries

The top surface of the domain (minus the jet BCs) is adiabatic. The lateral quadrilateral sides are open boundaries that permit the air to continue flowing outwardly. The bottom of the domain is an isothermal wall at 1,000 K. The swirling air flowing out the six jets eventually impinges the bottom surface, thereby transferring heat from the plate. The heated air at the surface of the hot plate is entrained by the swirling and mixing air above the plate. The calculations are conducted for θ = 0 (conventional jet), 5, 10, 15, 20, 25, 50, and 75° (S = 0,

0.058, 0.12, 0.18, 0.24, 0.31, 0.79, and 2.49, respectively). With the exception of varying the swirl angle, the calculations used the same mesh (L/D=3), Fuego CFD version (Fuego, 2009), and input. A similar set of calculations used L/D=12.

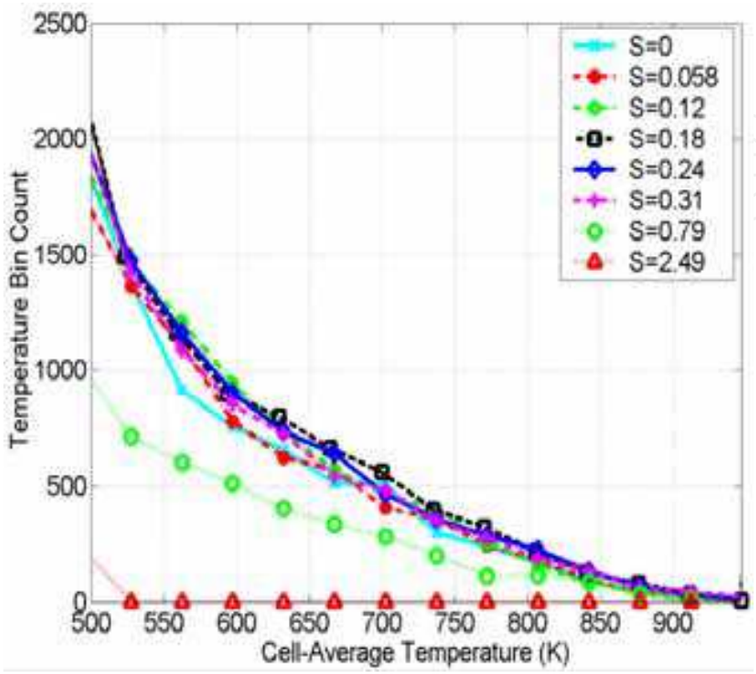

Fig. 14. Temperature Bin Count for All Elements with L/D = 12 Mesh

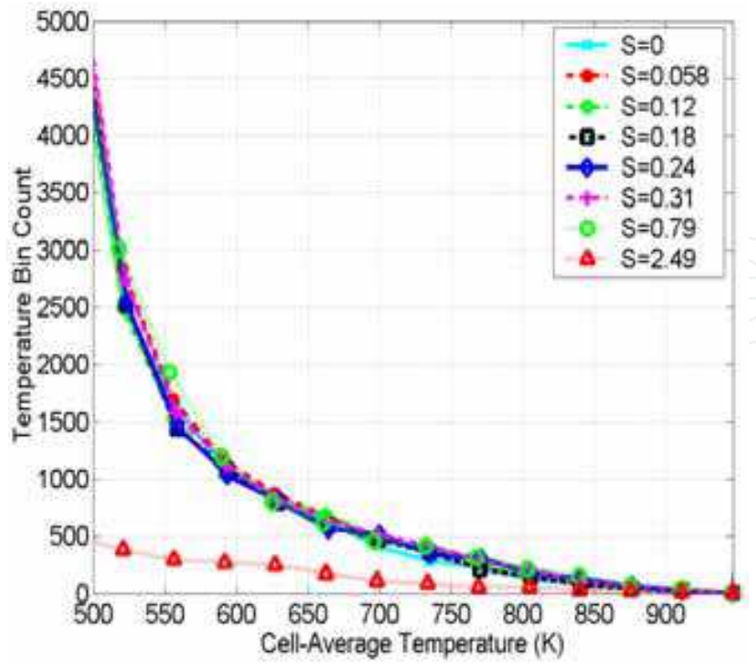

Fig. 15. Temperature Bin Count for All Elements with L/D = 3 Mesh

As a way to quantify S vs. cooling potential, all the hexahedral elements cell-averaged temperatures are grouped according to a linear temperature distribution ("bins"). The calculated temperature bins presented in Figures 14 and 15 show that at a given L/D and for S in a certain range, there are a higher number of hotter finite elements in the flow field. This is indicative of the swirling jet enhanced heat transfer ability over a conventional impinging jet to remove heat from the isothermal plate. For example, Figure 14 shows that for L/D = 12, and S ranging from 0.12 to 0.31, the swirling jets removed more heat from the plate, and thus are hotter than the impinging jet with S = 0. Additionally, the best cooling is achievable when S = 0.18. However, Figure 15 shows that for L/D = 3, and S ranging from 0.12 to 0.79, the swirling jets removed more heat from the plate, and are thus hotter than the impinging jet with S = 0. The best swirling jet cooling under these conditions is when S = 0.79. The results confirmed that for S ≤ 0.058, the flow field closely approximates the flow field for an impinging jet, S = 0, with insignificant enhancement to the heat transfer.

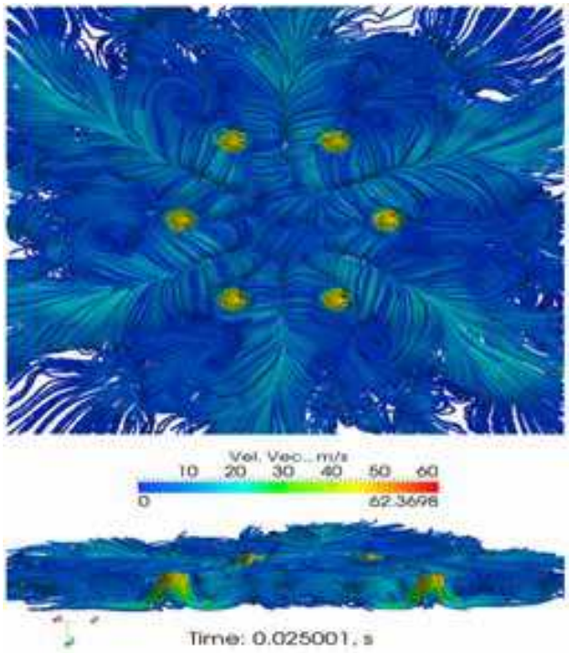

Fig. 16. Velocity Flow Field for the Mesh with L/D = 3 and S = 0.79. Top Image: Domain View of Top; Bottom Image: Domain Cross-Section

The back flow zone manifested as the CRZ appears to enhance the heat transfer compared to the swirling flow with no CRZ, as evidenced by the multiple-jet calculations shown in Figures 14 and 15. As noted previously, the azimuthal velocity of the swirling jet decays as $1/z^2$. Therefore, the largest heat transfer enhancement of the swirling occurs within a few jet diameters as evidenced by the results in Figures 14 and 15.

It is not surprising that the multiple swirling jets enhance cooling of the bottom isothermal plate only when the azimuthal velocity has not decayed before reaching the intended target (i.e. the isothermal plate in this case). The calculated velocity field for the swirling jet for L/D = 3 and S = 0.79 is shown in Figure 16. The upper insert in Figure 16 shows the velocity distribution at the top of the computation domain near the nozzle exit, while the bottom insert shows a cross-section view of the domain. The circulation roles appear as a result of

the interaction of the flow field by the multiple jets, rather than the value of S (the roles for S = 0.0 are very similar to those for S = 0.79). Note that the flow field shows that the jets impinge on the isothermal plate at velocities ranging from 25 to 35 m/s, which is a significant fraction of the initial velocity of 60 m/s. Thus, the azimuthal momentum is significant, inducing significant swirl that results in more mixing and therefore more cooling of the plate.

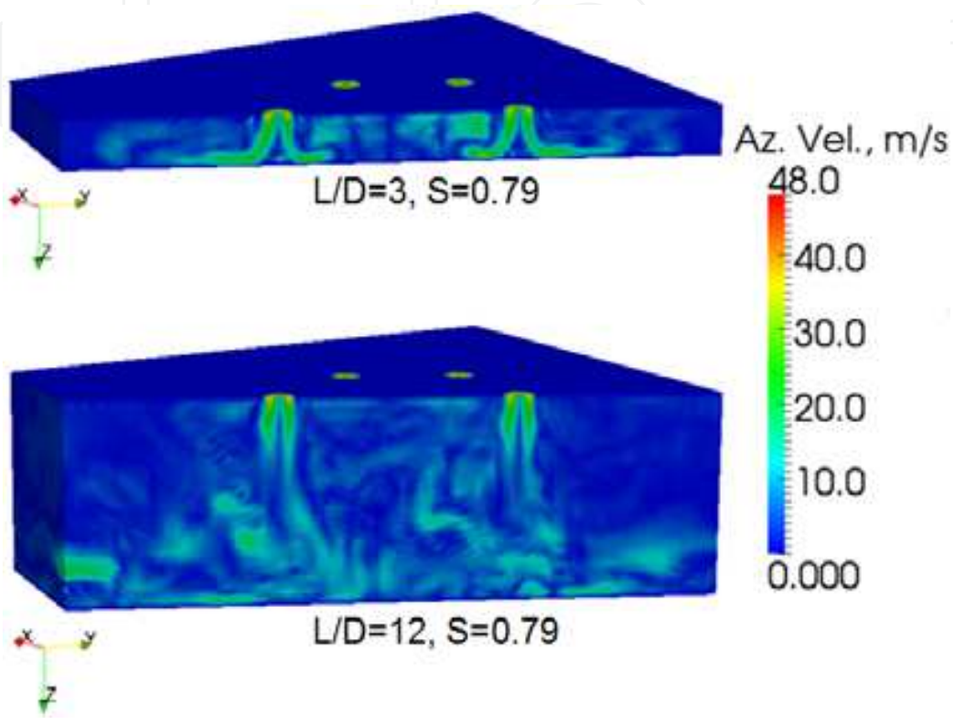

Fig. 17. Azimuthal Flow Field for S = 0.79. Top Image: L/D = 3; Bottom Image: L/D = 12

The high degree of enhanced cooling and induced mixing by swirling jets can be better understood by comparing the azimuthal flow fields shown in Figure 17 for S = 0.79 (the top has L/D = 3 and the bottom has L/D = 12). Note that for L/D = 3, the azimuthal velocity is approximately 25 to 35 m/s by the time it reaches the isothermal plate, but for the case with L/D = 12, the azimuthal velocity at the isothermal plate is 15 to 25 m/s. The calculated temperature field for S = 0.79 and L/D = 3 is shown in Figure 18. Thus, because the azimuthal velocity decays rapidly with distance from the nozzle exit, the value of L/D determines if there will be a significant azimuthal flow field by the time the jet reaches the isothermal bottom plate. Therefore, smaller L/D results in more heat transfer enhancement as S increases.

Results also show that the swirling jet flow field transitions to that of a conventional jet beyond a few jet diameters. For example, according to weak swirl theory, at L/D = 10, the swirling jet's azimuthal velocity decays to ~1% of its initial value, so the azimuthal momentum becomes negligible at this point; instead, the flow field exhibits radial and axial momentum, just like a conventional jet. Therefore, a free (unconstrained) swirling jet that becomes fully developed will eventually transition to a conventional jet, which is consistent with the recent similarity theory of Ewing (Semaan, Naughton, and Ewing, 2009). Clearly,

then, the advantages offered by the swirl are only available within a few jet diameters from the nozzle exit, depending on the value of S and Re.

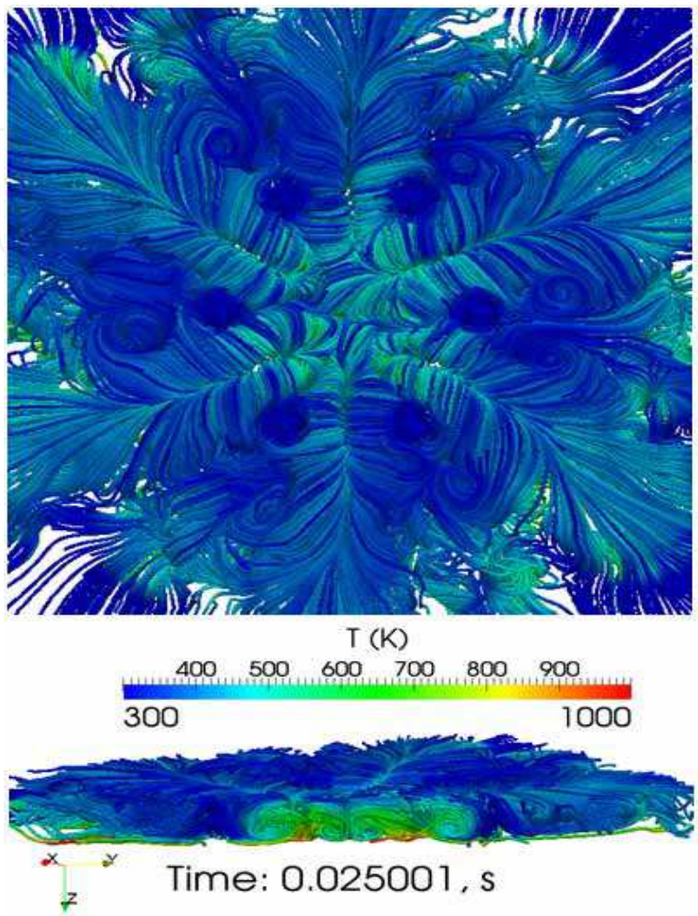

Fig. 18. Temperature Field for the Mesh with L/D = 3 and S = 0.79. Top Image: Domain View of Top; Bottom Image: Domain Cross-Section

7. Multiphysics, advanced swirling-jet LP modeling

For another application of swirling jets, calculations are performed for the LP of a prismatic core VHTR. The helium gas flowing in vertical channels cools the reactor core and exits as jets into the LP. The graphite blocks of the reactor core and those of the axial and radial reflectors are raised using large diameter graphite posts in the LP. These posts are structurally supported by a thick steel plate that is thermally insulated at the bottom. The issue is that the exiting conventional hot helium jets could induce hot spots in the lower support region, and together with the presence of the graphite posts, hinder the helium gas mixing in the LP chamber (Johnson and Schultz, 2009; McEligot and McCreery, 2004).
The performed calculation pertinent to these critical issues of operation safety of the VHTR included the following:

- Fuego-Calore coupled code,
- Helicoid vortex swirl model,

- Dynamic Smagorinsky large eddy simulation (LES) turbulence model,
- Participating media radiation (PMR),
- 1D conjugate heat transfer (CHT), and
- Insulation plate at the bottom of the LP.

The PMR model calculates the impact of radiation heat transfer for the high temperature helium gas behavior as a participating media. For the CHT, it is assumed that the LP wall conducts heat, which is subsequently removed by convection to the ambient fluid.

The full-scale, half-symmetry mesh used in the LP simulation had unstructured hexahedral elements and accounted for the graphite posts, the helium jets, the exterior walls, and the bottom plate with an insulating outer surface (Allen, 2004; Rodriguez and El-Genk, 2011). The impact of using various swirl angles on the flow mixing and heat transfer in the LP is investigated. For these calculations, the exit velocity for the conventional helium jets in the +z direction is V_0 = 67 m/s. The emerging gas flow from the coolant channels in the Cartesian x, y, and z directions has v_x, v_y, and v_z velocity components, respectively, whose magnitude depends on the swirl angle of the insert, θ, placed at the exit of the helium coolant channels into the LP. The initial time step used is 0.01 μs, and the simulation transient time is five to 25 s, with the CFL condition set to 1.0. In three helium jets (used as tracers), the temperature of the exiting helium gas is set to 1,473 K in order to investigate their tendency to form hot spots in the lower support plate and thermally-stratified regions in the LP; the exiting helium gas from the rest of the jets is at 1,273 K (Rodriguez and El-Genk, 2011). For these calculations S = 0.67.

Figure 19 shows key output from the coupled calculation, including the velocity streamlines (A), plate temperature distribution (B), fluid temperature as seen from the top (C), and fluid temperature shown from the bottom side (D). At steady state, Re in the LP ranges from 500 to 35,000. The lower RHS region in the LP experiences the lowest crossflow (Re ~ 500), as shown in Figure 19A. As a consequence of the low crossflow, the hot helium jet that exists strategically in that vicinity is able to reach the bottom plate with higher temperature (Figure 19B, RHS) than the other two tracer hot channels (LHS) that inject helium onto regions with much higher crossflow (Rodriguez and El-Genk, 2011). Consequently, Figure 19C shows that these two jets are unable to reach the lower plate. This is a basic effect of conventional jets in crossflow (Blevins, 1992; Chassaing *et al*., 1974; Goldstein and Behbahani, 1982; Kamotani and Greber, 1974; Kavsaoglu and Schetz, 1989; Kawai and Lele, 2007; Kiel *et al*., 2003; Patankar, Basu, and Alpay, 1977; Rivero, Ferre, and Giralt, 2001; Sucec and Bowley, 1976; Nirmolo, 1970; Pratte and Baines, 1967), and swirling jets in crossflow (Denev, Frohlich, and Bockhorn, 2009; Kamal, 2009; Kavsaoglu and Schetz, 1989): *the higher the ratio of crossflow velocity to the jet velocity, the faster the jet will bend in a parabolic profile.* Figure 19D shows the fluid temperature as seen from the bottom.

Figure 20 shows the velocity threshold for the three hot tracer helium flow channels. The results confirm that despite the fact that there are a total of 138 jets in the half-symmetry model of the VHTR LP, each jet follows a rather narrowly-defined path that widens two to seven times the initial jet diameter, and follows the classic parabolic trajectory of a jet in crossflow. Figure 21 shows the fluid temperature (based on thresholds) for the hot helium tracer channels. Due to the induced mixing, the helium gas temperature drops ~ 100 K within a few jet diameters from the channel exit. These figures allow the systematic tracing of velocity and temperature profiles of the three selected jets, without obstruction from other adjacent, cooler jets.

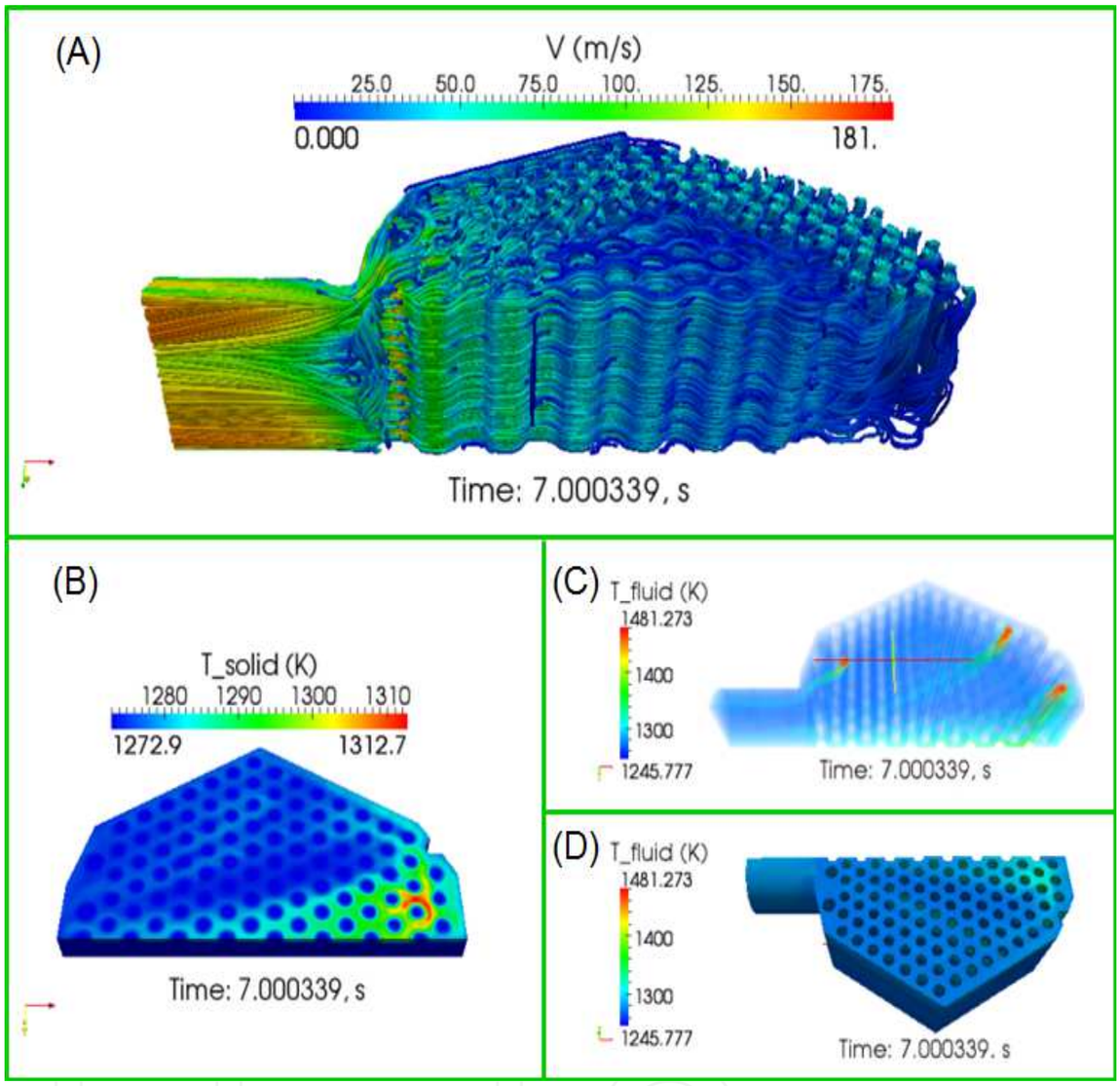

Fig. 19. Fuego-Calore Output Showing: (A) Velocity Streamlines. (B) Plate Temperature Distribution, (C) Volume Rendering of Fluid Temperature, and (D) Fluid Temperature at the Bottom Side

Calculations with S ranging from 0 to 2.49 were also conducted (Rodriguez and El-Genk, 2011). Note that for low S, there is less mixing in the region adjacent to the jet exit, but the jet is able to reach the bottom plate. Conversely, for higher S, there is more mixing near the jet exit, but significantly less of the jet's azimuthal momentum reaches the bottom plate. For a sufficiently large S and tall LP, the azimuthal momentum decays before reaching the bottom plate. The optimal height for swirling jets (with no crossflow) can be calculated via z, as discussed in Section 4.*

Figures 20 and 21 indicate that the jet penetration in the axial direction is a strong function of the crossflow. So, the lower the crossflow (RHS of said figures), the deeper the jets are able to penetrate, and vice-versa (LHS of said figures). Therefore, due to swirl decay and crossflow issues, S needs to be adjusted according to the local flow field conditions and desired LP height.

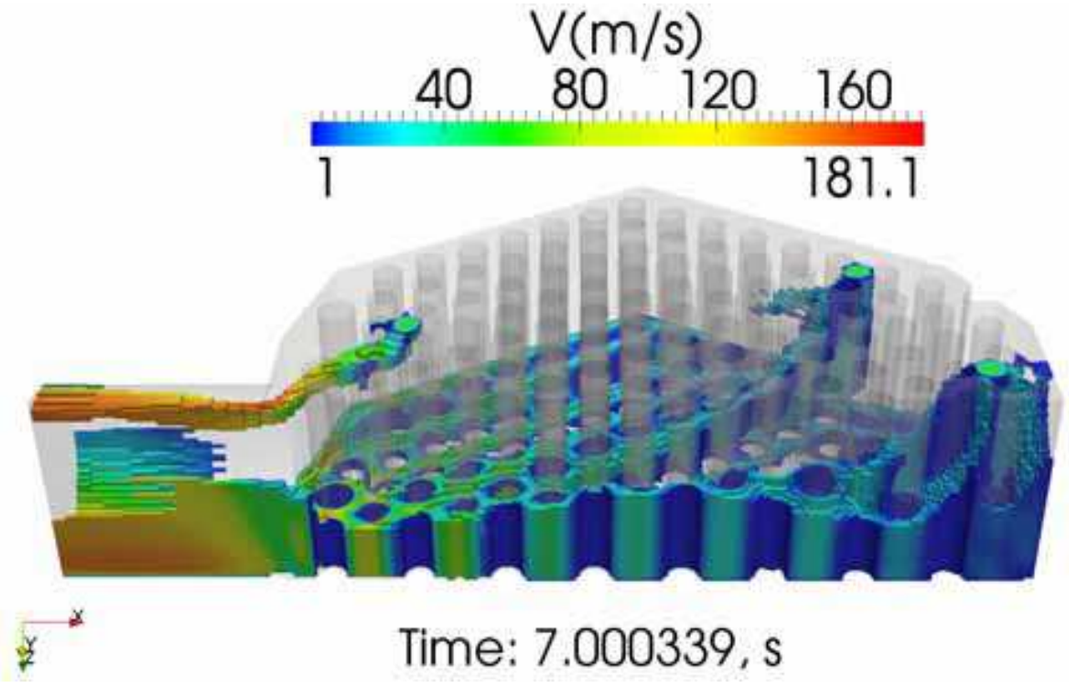

Fig. 20. Velocity Threshold for the Three Hot Channels

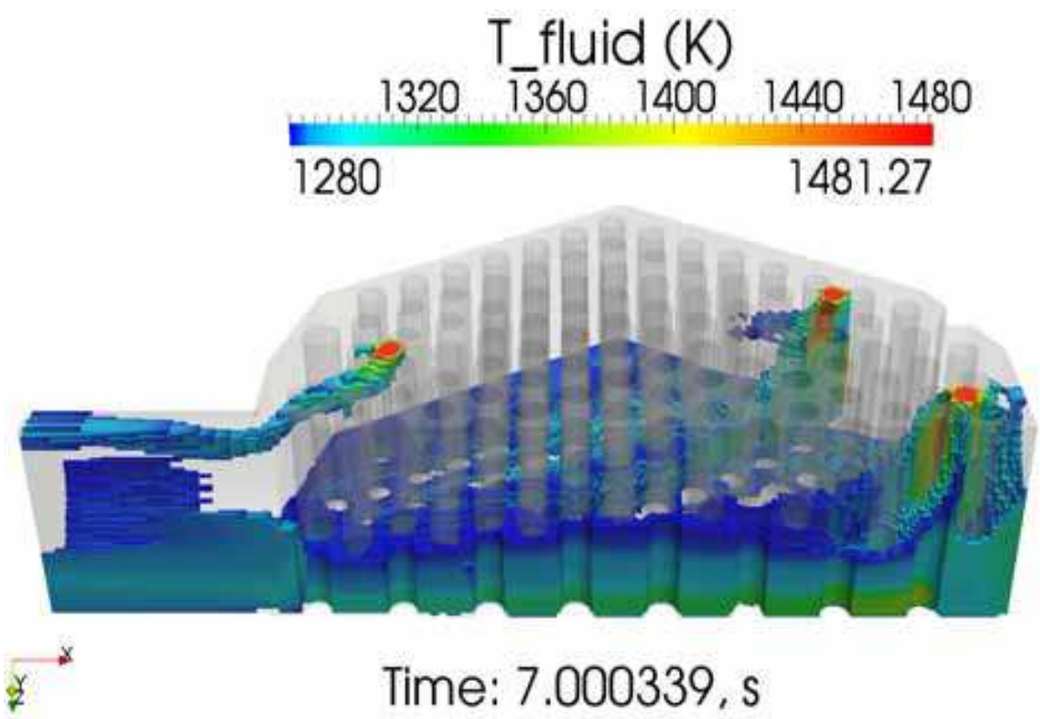

Fig. 21. Temperature Threshold for the Three Hot Channels

Figure 22 shows the bottom plate temperature. Note that the higher temperatures occur in areas of the LP where the helium gas jets are able to reach the bottom. Thus, the peak

temperature corresponds to the jet that impinges onto the region with the lowest Re (opposite end of the LP outlet). Figure 23 shows the convective heat transfer coefficient, h. Its magnitude is small, comparable to that of forced airflow at 2 m/s over a plate (Holman, 1990). Because the relatively low jet velocity near the LP bottom plate (0 - 20 m/s), the values for h ~ 2 to 12 W/m²K are reasonable. Note that h is zero (of course) in the region occupied by the support posts (shown as the large, dark blue circles).

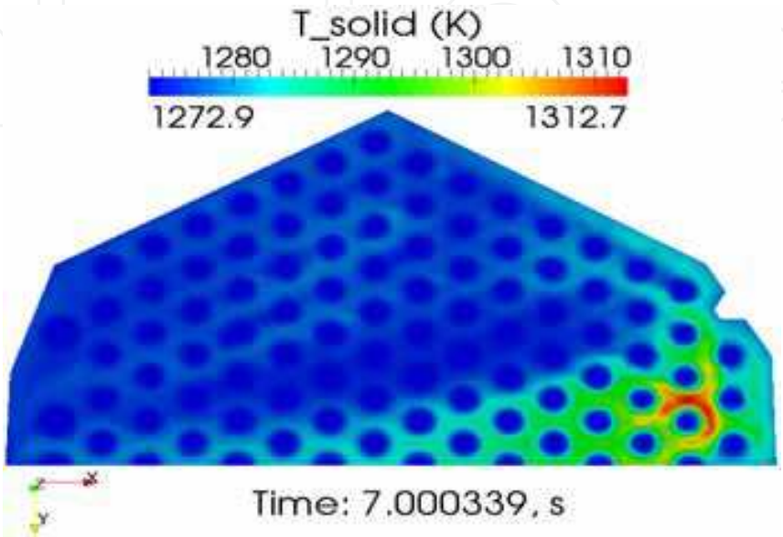

Fig. 22. Bottom Plate Temperature

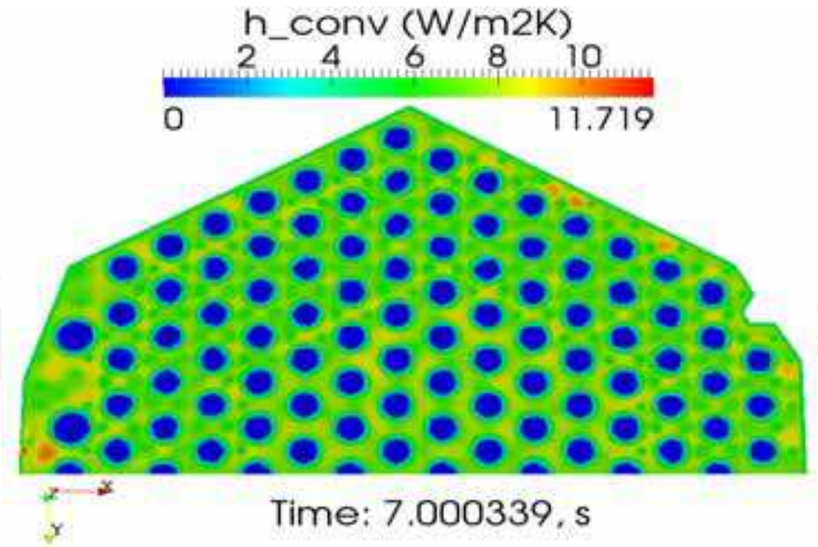

Fig. 23. Bottom Plate Heat Transfer Coefficient

The above figures confirm that swirling jets can mitigate thermal stratification and the formation of hot spots in the lower support plate in the VHTR LP. The mitigation of those two issues is achievable by adding swirl inserts at the exit of the helium coolant channels in the VHTR core, slightly increasing the pressure drop in the channels and across the LP. *An*

inspection of the pressure drop caused by the static helicoid device on a single, standalone helicoid shows that there was a relatively small drop of approximately 1,000 Pa (0.15 psi), as shown in Figure 24. This result is consistent with those found in the literature for hubless swirlers (Mathur and MacCallum, 1967). Given the benefits related to enhanced mixing and turbulence gained as a result of the swirling device, such small pressure drop is clearly justified.

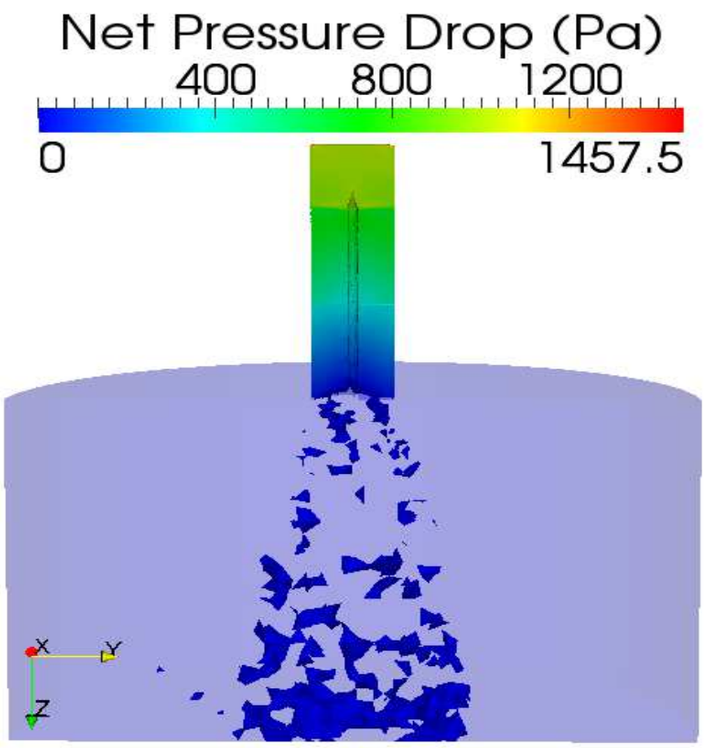

Fig. 24. Net Pressure Drop Across Helicoid Geometry

8. Conclusion

A helicoid vortex swirl model, along with the Fuego CFD and Calore heat transfer codes are used to investigate mixing and heat transfer enhancements for a number of swirling jet applications. Critical parameters are S, CRZ, swirl decay, jet separation distance, and Re. As soon as the CRZ forms, the azimuthal velocity field for the swirling jets does not travel as far, even when Re increases substantially. For example, once the CRZ develops, a 10-fold increase in Re has a smaller impact on the flow field than S.

Knowing at a more fundamental level how vortices behave and what traits they have in common allows for insights that lead to vortex engineering for the purpose of maximizing heat transfer and flow mixing. Because the CRZ is a strong function of the azimuthal and axial velocities, shaping those velocity profiles substantially affect the flow field.

As applications for the material discussed herein, simulations are performed for: (1) unconfined jet, (2) jets impinging on a flat plate, and (3) a VHTR LP. The calculations show the effects of S, CRZ, L/D, swirl decay, and Re. For the VHTR LP calculations, results demonstrated that hot spots and thermal stratification in the LP can be mitigated using swirling jets, while producing a relatively small pressure drop.

9. References

Aboelkassem, Y., Vatistas, G. H., and Esmail, N. (2005). Viscous Dissipation of Rankine Vortex Profile in Zero Meridional Flow, *Acta Mech. Sinica*, Vol. 21, 550 – 556

Allen, T. (2004). Generation IV Systems and Materials, Advanced Computational Materials Science: Application to Fusion and Generation-IV Fission Reactors, U. of Wisconsin

Batchelor, G. K. (1964). Axial Flow in Trailing Line Vortices, *J. Fluid Mech*., Vol. 20, Part 4, 645 – 658

Billant, P., Chomaz, J.-M., and Huerre, P. (1998). Experimental Study of Vortex Breakdown in Swirling Jets, *J. Fluid Mech*., Vol. 376, 183 – 219

Bird, R., Stewart, W., and Lightfoot, E. (2007). *Transport Phenomena*, John Wiley & Sons, 2nd Edition

Blevins, R. (1992). *Applied Fluid Dynamics Handbook*, Krieger Publishing Co., Florida

Burgers, J. M. (1948) *Advances in Applied Mechanics*, Vol. 1, Academic Press, New York, 171

Chassaing, P. *et al*. (1974). Physical Characteristics of Subsonic Jets in a Cross-Stream, *J. Fluid Mech.*, Vol. 62, Part 1, 41 – 64

Chepura, I. B. *et al*. (1969). On the Tangential Component of the Velocity Field in a Smooth-Wall Vessel Equipped with a Radial-Blade Mixer, *Teoreticheskie Osnovy Khimichesko i Tekhnologii*, Vol. 3, No. 3, 404 – 411

Chigier, N. A. and Chervinsky, A. (1967). Experimental Investigation of Swirling Vortex Motion in Jets, *ASME J. Applied Mechanics*, Series E, Vol. 3, 443 – 451

CUBIT, (2009). www/cs.sandia.gov/capabilities/CubitMeshingProgram/index.html

Denev, J. A., Frohlich, J., and Bockhorn, H. (2009). Large Eddy Simulation of a Swirling Transverse Jet into a Crossflow with Investigation of Scalar Transport, *Physics of Fluids*, Vol. 21, 015101

Duwig, C. *et al*. (2005). Large Eddy Simulation of a Swirling Flame Response to Swirl Modulation with Impact on Combustion Stability, 43rd AIAA Aerospace Sciences Meeting and Exhibit, AIAA 2005-1275, Reno, Nevada, January 10-13

Fuego (2009). SIERRA/Fuego Theory Manual – 4.11, Sandia National Laboratories

Fujimoto, Y., Inokuchi, Y., and Yamasaki, N. (2005). Large Eddy Simulation of Swirling Jet in Bluff-Body Burner, *J. Thermal Science,* Vol. 14, No. 1, 28 – 33

Garcia-Villalba, M., Frohlich, J., and Rodi, W. (2005). Large Eddy Simulation of Turbulent Confined Coaxial Swirling Jets, *Proc. Appl. Math. Mech*., Vol. 5, 463 – 464

Gol'Dshtik, M. A. and Yavorskii, N. I. (1986). On Submerged Jets, *Prikl. Matem. Mekhan*. USSR, Vol. 50, No. 4, 438 – 445

Goldstein, R. J. and Behbahani, A. I. (1982). Impingement of a Circular Jet with and without Cross Flow, *Int. J. Heat Mass Transfer*, Vol. 25, No. 9, 1377 – 1382

Gortler, H. (1954). Decay of Swirl in an Axially Symmetrical Jet, Far from the Orifice, *Revista Matematica Hispano-Americana*, Vol. 14, 143 – 178

Huang, L. (1996). Heat Transfer and Flow Visualization of Conventional and Swirling Impinging Jets, Ph.D. Diss., University of New Mexico

Huang, L. and El-Genk, M. (1998). Heat Transfer and Flow Visualization Experiments of Swirling, Multi-Channel, and Conventional Impinging Jets, *Int. J. Heat Mass Transfer*, Vol. 41, No. 3, 583 – 600

Hwang, W.-S. and Chwang, A. T. (1992). The Swirling Round Laminar Jet, *J. of Engineering Mathematics*, Vol. 26, 339 – 348

Johnson, G. A. (2008). Power Conversion System Evaluation for the Next Generation Nuclear Plant (NGNP), Proc. International Congress on Advances in Nuclear Power Plants (ICAPP 08), American Nuclear Society, Paper 8253, Anaheim, CA

Johnson, R. W. and Schultz, R. R. (2009). Computational Fluid Dynamic Analysis of the VHTR Lower Plenum Standard Problem, INL/EXT-09-16325, Idaho Nat. Lab.

Kamal, M. M. (2009). Combustion in a Cross Flow with Air Jet Nozzles, *Combust. Sci. and Tech.*, Vol. 181, 78 – 96

Kamotani, Y. and Greber, I. (1974). Experiments on Confined Turbulent Jets in Cross Flow, NASA CR-2392

Kavsaoglu, M. S. and Schetz, J. A. (1989). Effects of Swirl and High Turbulence on a Jet in a Crossflow, *J. Aircraft*, Vol. 26, No. 6, 539 – 546

Kawai, S. and Lele, S. K. (2007). Mechanisms of Jet Mixing in a Supersonic Crossflow: A Study Using Large-Eddy Simulation, Center for Turbulence Research, Annual Research Briefs, 353 – 365

Kiel, B. *et al*. (2003). Experimental Investigation of Vortex Shedding of a Jet in Crossflow, 41st Aerospace Sciences Meeting and Exhibit, AIAA 2003-182, Reno, Nevada

Kim, M.-H., Lim, H.-S, and Lee, W.-J. (2007). A CFD Analysis of a Preliminary Cooled-Vessel Concept for a VHTR, Korea Atomic Energy Research Institute

Lamb, H. (1932). *Hydrodynamics*, 6th Ed., Cambridge Univ. Press

Larocque, J. (2004). Heat Transfer Simulation in Swirling Impinging Jet, Institut National Polytechnique de Grenoble, Division of Heat Transfer

Laurien, E., Lavante, D. v., and Wang, H. (2010). Hot-Gas Mixing in the Annular Channel Below the Core of High-Power HTR's, Proceedings of the 5th Int. Topical Meeting on High Temperature Reactor Technology, HTR 2010-138, Prague, Czech Republic

Lavante, D. v. and Laurien, E. (2007). 3-D Simulation of Hot Gas Mixing in the Lower Plenum of High-Temperature Reactors, *Int. J. for Nuclear Power*, Vol. 52, 648 – 649

Loitsyanskiy, L. G. (1953). The Propagation of a Twisted Jet in an Unbounded Space Filled with the Same Fluid, *Prikladnaya Matematika i Mekhanika*, Vol. 17, No. 1, 3 – 16

Martynenko, O. G., Korovkin, V. N., and Sokovishin, Yu. A. (1989). A Swirled Jet Problem, *Int. J. Heat Mass Transfer*, Vol. 32, No. 12, 2309 – 2317

Mathur, M. L. and MacCallum, N. R. L. (1967). Swirling Air Jets Issuing from Vane Swirlers. Part 1: Free Jets, *Journal of the Institute of Fuel*, Vol. 40, 214 – 225

McEligot, D. M. and McCreery, G. E. (2004). Scaling Studies and Conceptual Experiment Designs for NGNP CFD Assessment, Idaho National Engineering and Environment Laboratory, INEEL/EXT-04-02502

Nematollahi, M. R. and Nazifi, M. (2007). Enhancement of Heat Transfer in a Typical Pressurized Water Reactor by New Mixing Vanes on Spacer Grids, ICENES

Newman, B. G. (1959). Flow in a Viscous Trailing Vortex, *The Aero. Quarterly*, 149 – 162

Nirmolo, A. (2007). Optimization of Radial Jets Mixing in Cross-Flow of Combustion Chambers Using Computational Fluid Dynamics, Ph.D. Diss., Otto-von-Guericke U. of Magdeburg, Germany

Patankar, S. V., Basu, D. K., and Alpay, S. A. (1977). Prediction of the Three-Dimensional Velocity Field of a Deflected Turbulent Jet, *J. of Fluids Engineering*, 758 – 762

Pratte, B. D. and Baines, W. D. (1967). Profiles of Round Turbulent Jets in a Cross Flow, Procs. of the American Society of Civil Engineers, *J. Hydraulics Div*., Vol. 92, 53 – 64

Rankine, W. J. (1858). *A Manual of Applied Mechanics*, 9th Ed., C. Griffin and Co., London, UK

Rivero, A., Ferre, J. A., and Giralt, F. (2001). Organized Motions in a Jet in Crossflow, *J. Fluid Mech.*, Vol. 444, 117 – 149

Rodriguez, S. B. and El-Genk, M. S. (2008a). Using Helicoids to Eliminate 'Hot Streaking' and Stratification in the Very High Temperature Reactor Lower Plenum, *Proceedings of ICAPP '08*, American Nuclear Society, Paper 8079, Anaheim, CA

Rodriguez, S. B. and El-Genk, M. S. (2008b). On Eliminating 'Hot Streaking' and Stratification in the VHTR Lower Plenum Using Helicoid Inserts, *HTR-08*, American Society of Mechanical Engineers, Paper 58292, Washington, DC

Rodriguez, S. B., Domino, S., and El-Genk, M. S. (2010). Safety Analysis of the NGNP Lower Plenum Using the Fuego CFD Code, CFD4NRS-3 Workshop, Experimental Validation and Application of CFD and CMFD Codes to Nuclear Reactor Safety Issues, Washington, DC

Rodriguez, S. B. and El-Genk, M. S. (2010a). Numerical Investigation of Potential Elimination of 'Hot Streaking' and Stratification in the VHTR Lower Plenum using Helicoid Inserts, *Nuclear Engineering and Design Journal*, Vol. 240, 995 – 1004

Rodriguez, S. B. and El-Genk, M. S. (2010b). Cooling of an Isothermal Plate Using a Triangular Array of Swirling Air Jets, *14th Int. Heat Transfer Conference*, Wash. DC

Rodriguez, S. B. and El-Genk, M. S. (2010c). On Enhancing VHTR Lower Plenum Heat Transfer and Mixing via Swirling Jet, *Procs. of ICAPP 10,* Paper 10160, S. Diego, CA

Rodriguez, S. B. and El-Genk, M. S. (2010d). Heat Transfer and Flow Field Characterization of a Triangular Array of Swirling Jets Impinging on an Adiabatic Plate, *Proc. 14th Int. Heat Transfer Conference*, Washington DC

Rodriguez, S. B. and El-Genk, M. S. (2011). Coupled Computational Fluid Dynamics and Heat Transfer Analysis of the VHTR Lower Plenum, Proceedings of ICAPP-11, Paper 11247, Nice, France

Semaan, R., Naughton, J., and Ewing, F. D. (2009). Approach Toward Similar Behavior of a Swirling Jet Flow, 47th AIAA Aero. Sc. Mtg., Orlando, Florida, Paper 2009-1114

Smagorinsky, J. (1963). General Circulation Experiments with the Primitive Equations I. The Basic Experiment, Dept. of Com., *Monthly Weather Rep.*, Vol. 91, No. 3, 99 – 164

Squire, H. B. (1965). The Growth of a Vortex in a Turbulent Flow, *The Aeronautical Quarterly*, Vol. 16, Part 1, 302 – 306

Sucec, J. and Bowley, W. W. (1976). Prediction of the Trajectory of a Turbulent Jet Injected into a Crossflowing Stream, *J. of Fluids Engineering*, 667 – 673

Sullivan, R. D. (1959). A Two-Cell Vortex Solution of the Navier-Stokes Equations, *J. of the Aerospace Sciences*, Vol. 26, No. 11, 767 – 768

Taylor, G. I. and Green, A. E. (1937). Mechanism of the Production of Small Eddies from Large Ones, *Proceedings of the Royal Society of London, Series A, Mathematical and Physical Sciences*, Vol. 158, No. 895, 499 – 521

Tsukker, M. S. (1955). A Swirled Jet Propagating in the Space Filled with the Same Fluid, *Prikladnaja Matematika i Mehanika*, Vol. 19, No. 4, 500 – 503

Watson, E. A. and Clarke, J. S. (1947). Combustion and Combustion Equipment for Aero Gas Engines, *J. Inst. Fuel*, Vol. 21, 572 – 579

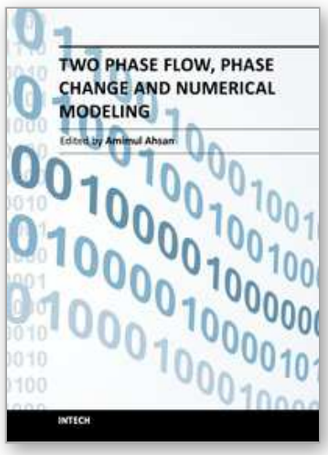

Two Phase Flow, Phase Change and Numerical Modeling
Edited by Dr. Amimul Ahsan

ISBN 978-953-307-584-6
Hard cover, 584 pages
Publisher InTech
Published online 26, September, 2011
Published in print edition September, 2011

The heat transfer and analysis on laser beam, evaporator coils, shell-and-tube condenser, two phase flow, nanofluids, complex fluids, and on phase change are significant issues in a design of wide range of industrial processes and devices. This book includes 25 advanced and revised contributions, and it covers mainly (1) numerical modeling of heat transfer, (2) two phase flow, (3) nanofluids, and (4) phase change. The first section introduces numerical modeling of heat transfer on particles in binary gas-solid fluidization bed, solidification phenomena, thermal approaches to laser damage, and temperature and velocity distribution. The second section covers density wave instability phenomena, gas and spray-water quenching, spray cooling, wettability effect, liquid film thickness, and thermosyphon loop. The third section includes nanofluids for heat transfer, nanofluids in minichannels, potential and engineering strategies on nanofluids, and heat transfer at nanoscale. The forth section presents time-dependent melting and deformation processes of phase change material (PCM), thermal energy storage tanks using PCM, phase change in deep CO2 injector, and thermal storage device of solar hot water system. The advanced idea and information described here will be fruitful for the readers to find a sustainable solution in an industrialized society.

How to reference
In order to correctly reference this scholarly work, feel free to copy and paste the following:

Sal B. Rodriguez and Mohamed S. El-Genk (2011). Recent Advances in Modeling Axisymmetric Swirl and Applications for Enhanced Heat Transfer and Flow Mixing, Two Phase Flow, Phase Change and Numerical Modeling, Dr. Amimul Ahsan (Ed.), ISBN: 978-953-307-584-6, InTech, Available from: http://www.intechopen.com/books/two-phase-flow-phase-change-and-numerical-modeling/recent-advances-in-modeling-axisymmetric-swirl-and-applications-for-enhanced-heat-transfer-and-flow-

INTECH
open science | open minds

InTech Europe
University Campus STeP Ri
Slavka Krautzeka 83/A
51000 Rijeka, Croatia
Phone: +385 (51) 770 447
Fax: +385 (51) 686 166
www.intechopen.com

InTech China
Unit 405, Office Block, Hotel Equatorial Shanghai
No.65, Yan An Road (West), Shanghai, 200040, China
中国上海市延安西路65号上海国际贵都大饭店办公楼405单元
Phone: +86-21-62489820
Fax: +86-21-62489821

IntechOpen